The 6th IBPSA Canada Conference
La 6e conférence d'IBPSA – Canada
Winnipeg, May 19 – 20

PREDICTION OF LOCAL HEAT TRANSFER IN A VERTICAL CAVITY USING ARTIFICIAL NEURAL NETWORK

M. Ebrahim Poulad, D. Naylor, A. S. Fung
Department of Mechanical & Industrial Engineering
Ryerson University, Toronto

ABSTRACT

A time-averaging technique was developed to measure the unsteady and turbulent free convection heat transfer in tall vertical enclosure using a Mach-Zehnder interferometer. The method used a combination of digital high speed camera and an interferometer to obtain the time-averaged heat transfer rates in the cavity. The measured values were used to train an Artificial Neural Network (ANN) algorithm to predict the local heat transfer. The time-averaged local Nusselt number is needed to study local phenomena, e.g. condensation in windows (Wright, 1998); (Abodahab & Muneer, Feb. 1998).

Optical heat transfer measurements were made in a differentially heated vertical cavity with isothermal walls. The cavity widths (distance between the plates) were W = 12.7, 32.3, 40, and 56.2mm. The corresponding Rayleigh numbers were about $3x10^3$, $5x10^4$, $1x10^5$, $2.7x10^5$, respectively, and the enclosure aspect ratio (H/W) ranged from A=18 to 76. The fluid was air and the temperature differential was about 15 K for all measurements.

Alyuda NeuroIntelligence 2.2 (577) software (Alyuda Research Inc., 2003) is used to generate solutions for the time-averaged local Nusselt number in the cavity based on the experimental data. Here, feed-forward architecture and trained by Levenberg- Marquardt (LM) algorithm is adopted. The ANN is designed to suit the present system which has 4 to 13 inputs and 1 output. The network predictions are found to be in a good agreement with the experimental observed value of local Nusselt number.

INTRODUCTION

Architects and building designers are not supposed to be well knowledgeable in Computational Fluid Dynamics (CFD) and complicated mathematical equations solving techniques to understand the heat transfer inside the double glazed windows, but they love to have a tool to give them a reasonable idea of what would be the impact of their design on the natural phenomena. Condensation of the water on the window due to the humidity of the air is an interested phenomenon. Condensation happens because of the heat transfer between window and humid air at that level. This is a complicated process for non-mechanical engineers. This paper aims to train a NN based on experimental data to predict the heat transfer at different levels. Therefore it would be easy to use this trained NN to predict the heat transfer by just interring the physical conditions (e.g. temperature and size of the window). (Abodahab & Muneer, Feb. 1998) measured the longitudinal temperature along double glazed window to investigate the condensation occurrence. They developed a model that takes four inputs (internal temperature, external temperature, U-value of the window and indoor relative humidity to determine the risk of condensation.

In recent years, there has been a renaissance of interest in interferometry, in part because of the rapid developments in computer modeling of heat transfer. In the current study, measurements of free convection have been made in a tall air-filled vertical enclosure. Figure 1 shows the test geometry and the three dimensional coordinate system. The enclosure consisted of two differentially heated plates, which were temperature controlled using constant temperature baths. The side walls that sealed the enclosure were machined from acrylic. This geometry was chosen because the flow regimes are well known.

The current optical method uses the beam-averaged temperature field to measure the instantaneous and time-averaged convective heat transfer rates.

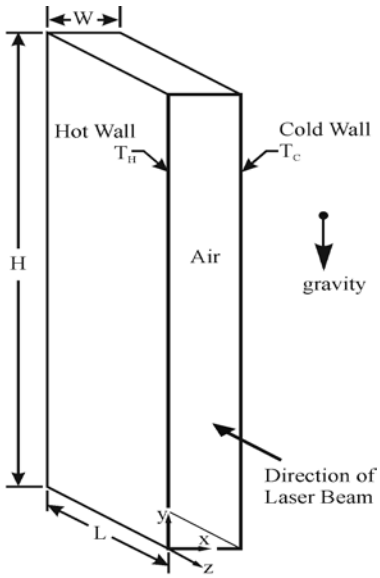

Figure 1: Experimental geometry and coordinate system.

The interference fringe pattern in the output of the interferometer results from the spatial integration of

changes in the refractive index of the test fluid (air). As shown in Figure 1, the refractive index of the test fluid, $n(x,y,z,t)$, is integrated along the path of the laser light beam from the inlet to the outlet of the model. The instantaneous fringe shift, $\varepsilon(x,y,t)$, is related to the temperature field, $T(x,y,z,t)$, as follows:

$$\varepsilon(x,y,t) = \frac{1}{\lambda_o}\int_0^L \left[n_{ref} - n(x,y,z,t)\right]dz$$

$$= \frac{PG}{R\lambda_o}\int_0^L \left(\frac{1}{T_{ref}} - \frac{1}{T(x,y,z,t)}\right)dz \qquad (1)$$

where L is the length of the experimental model in the light beam direction, P is the absolute pressure, G is the Gladstone-Dale constant, R is the gas constant, and λ_o is the vacuum wavelength of the He-Ne laser light source. The fringe shift order is measured relative to a surface with a known temperature, T_{ref}.

The beam-averaged temperature gradient, normal to the measurement surface, was used to calculate the local convective heat flux. This was obtained by differentiating Eq.(1) with respect to x and applying the result at the surface (x=0). After some manipulation, it can be shown that the instantaneous local convective heat flux can be expressed as:

$$q_y^{"} = -k_s \left.\frac{\overline{\partial T}}{\partial x}\right|_{x=0} = -\frac{k_s R \lambda_o T_s^2}{LPG}\left.\frac{\partial \varepsilon}{\partial x}\right|_{x=0} \qquad (2)$$

where k_s is the fluid thermal conductivity, evaluated at the surface temperature. Eq. (2) has been used to evaluate the instantaneous local heat flux at each time interval, using the surface fringe shift gradient $(\partial\varepsilon/\partial x\,|_{x=0})$ measured in each interferogram. The instantaneous local Nusselt number (Nu_y) for the enclosure can be defined as:

$$Nu_y = \frac{h_y W}{k_f} = \frac{q_y^{"} W}{k_f\,(T_h - T_c)} \qquad (3)$$

where k_f is the conductivity of the test fluid (air) at film temperature, i.e. $(T_h + T_c)/2$. The details of this technique were published in SBRN conference proceedings (Poulad, Naylor, & Oosthuizen, June 25–27, 2009).

One hundred and fifty experiments implemented to measure time-averaged local Nusselt number on four different sizes. A combination of high speed digital camera and Mach-Zehnder interferometer (MZI) were used to record the interferograms, and then those input were used to calculate Nu_y. Figure 2 shows the steps of the experimental process. As the figure shows (step 6), the MATLAB Image Processing Toolbox was used to process images.

Due to the diffraction, interferometry cannot measure heat transfer at the surface, x=0, as Eq. (2) requirement is. Another problem with the MZI, it is expensive and like all measurement, there is some (about 5%) uncertainty into the calculations. Also, when the fringes are very wide or fine the measurement is not accurate (Poulad, 2009). Therefore, ANN is a good option to predict the local heat transfer.

During experiments, about 153 GB data were gathered from processing of 162,160 interferograms. The digital images were shaded from 0 (dark) to 255 (bright or saturated). The number of data for 12.7, 32.3, 40 and 56.2 size is 28, 25, 20 and 61, respectively. These data are used to train an Artificial Neural Network here.

The ANN has been using to optimize solar energy utilization and prediction of residential buildings energy consumption, e.g., (Aydinalp, Ugursal, & Fung, 2003) since a few decades ago. (Kalogirou & Bojic, 2000) used the ANN in the field of solar energy. He found that ANN can be used in other field of energy transformation and use too.

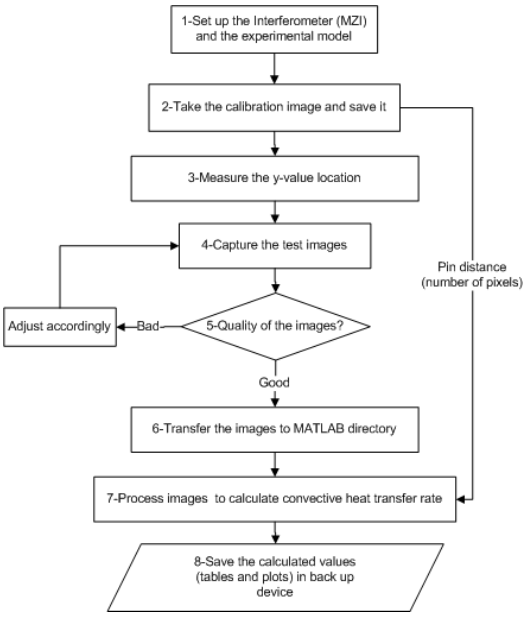

Figure 2: Steps in the current experiment to calculate Nusselt number

Artificial intelligence (AI) has two major branches, ANN and expert systems. During the last decade, there has been a substantial increase in interest concerning ANNs. They operate like a "black box" model; no detailed information about the system is required. They are huge parallel distributed processors that have a natural tendency for storing experimental knowledge and making it available for use. They work like the human brain in two ways, the network through a learning process takes the knowledge, and weight

(inner-neuron connection strengths) it to store the knowledge. They are able to learn from the experiments results, fault tolerant, able to handle incomplete and noisy data, able to deal with non-linear problems, and once they are trained, they can provide prediction and generalization at high speed and low cost (Gouda, Danaher, & Underwood, 2002). The network usually has an input layer, some hidden layers and an output layer. Simply, each neuron is connected to all the others of previous layer via adaptable weights. As knowledge is stored as a set of connection weight, during training, the connection weights are modified. The network uses a learning mode that the input is presented to the network along with the desired output. The weights are adjusted so that the network tries to produce the desired output. The weights, after training, contain meaningful information whereas before training they are random and have no meaning. Alyuda NeuroIntelligence 2.2 (577) software is used for simulation in this work.

Prediction of heat transfer by using ANN based on the experimental data is popular in the literature, e.g., (Ravindranath, Prabhukumar, & Devaru, 2007). With the best of knowledge of the authors, this is the first time ANN is used to predict the local Nusselt number in the cavity. ANN has been receiving an increasing attention for simulating engineering systems due to some interesting characteristics such as learning capability, fault tolerance, and non-linearity.

METHODOLOGY

To get the data for training the ANN, the MZI was set up first. It is shown schematically in Figure 3. It consists of the following pieces as numbered in the Figure 1) He-Ne laser (10mW, λ=632.8nm), 2&5) First surface mirror (flatness λ/10), 3&6) Beam splitter (50/50, parallelism 1 arc second, flatness λ/10), 4) Parabolic mirror (focal length of 64"), 7) Spherical mirror (focal length of 24"), 8) Small flat mirror (9x9 mm^2), and 9) High speed digital camera (CCD).

The solid arrow, in the Figure 3, demonstrates the path of collimated x-ray. A Helium-Neon laser, equipped with spatial filter and beam expander, was used as the source of monochromatic light to produce the interferograms. The expanded and collimated beam was separated into two equal beams after passing the beam splitter (item #3). These beams have the same phase because they are produced from same origin. One beam passes through ambient air while the other beam passes through the experimental model (cavity). The temperature of the experimental domain, which is different from ambient, changes the air density. This causes a change in the index of refraction. The change of index of refraction relative to the ambient beam creates a phase shift. This phase shift appears as constructive and destruction fringes when the two beams recombine at the second beam splitter (item #6). For the MZI shown in the Figure 3, the final recombined beam is focused in order to be photographed by the digital camera (item #9). The output, which is called an *interferogram*, was captured digitally.

The high speed camera (model: MotionPro X3) was made by Integrated Design Inc., USA. To get the maximum possible intensity, the lens was removed from camera and images were exposed directly on the camera sensors. In this way, in a single session the camera was able to capture a maximum area of approximately $\Delta y = 20$ mm by $\Delta x = 18$ mm on the experimental model. To view the entire model, the camera's "window" was moved within the interferometer beam. Figure 4 shows the camera mounted on a precision x-y-z positioning holder. Primary investigation showed that ten second capturing image with frequency of 100 Hz provides acceptable results. So far, the methodology of the experiments was introduced. Now, the specification or architecture of the ANN is described. Artificial neural networks are the simple clustering of the primitive artificial neurons.

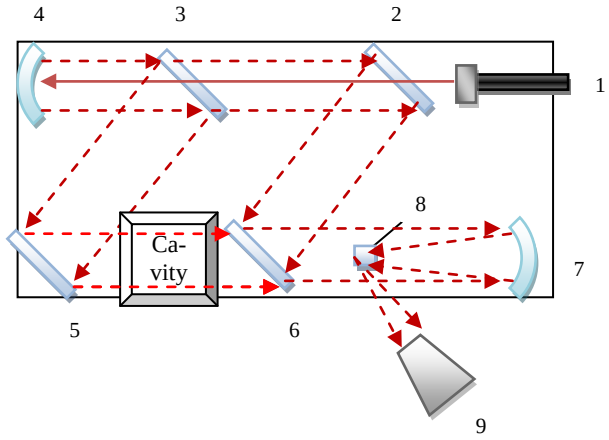

Figure 3: Plan view of a Mach-Zehnder interferometer

Figure 4: The camera holder equipped with micrometers in x, y and z direction.

This clustering occurs by creating layers, which are then connected to one another. How these layers connect may also vary. Originally, all artificial neural networks have a similar structure of topology. As the Figure 5 shows, the neurons are grouped into three layers. The input layer consists of neurons that receive input from the external environment. The output layer consists of neurons that communicate the output of the system to the user or external environment. There are usually a number of hidden layers between these two layers; the Figure 5 shows a simple structure with only one hidden layer.

In the Architecture Design of the NeuroIntelligence, user may manually enter a number of hidden layers (up to 5) and a number of hidden units in each layer (up to 256). By default, NeuroIntelligence proposes a topology with one hidden layer and with the number of hidden units equal to the number of inputs divided by 2. This maybe the best choice in some cases and authors run a search method with different architectures manually, and then the result was compared with the architecture proposed automatically by the NeuroIntelligence.

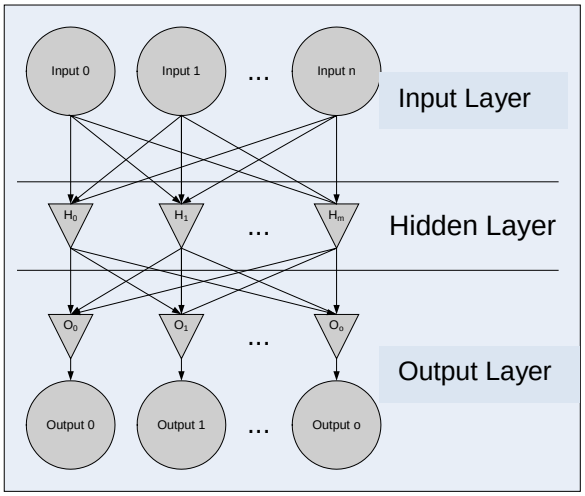

Figure 5: The structure of an ANN

When the input layer receives the input its neurons produce output, which becomes input to the other layers of the system. The process continues until a certain condition is satisfied or until the output layer is invoked and fires their output to the external environment. Figure 6 shows the fundamental elements of an ANN.

Alyuda shows the structure as n-m_1-…-m_k-u, which all of them are scalar numbers, n is the number of inputs, k is the number of hidden layers, m_i is the number of neurons in i^{th} layer, and u is the number of outputs. For example, 9-23-1 means a structure of 9 inputs, 23 neurons in one hidden layer and one output. By default, NeuroIntelligence divides each dataset onto three sets: the Training set (Tr), the Validation set (Va) and the Test set (Te).

Understanding Input Feature Selection

Input feature selection methods are used to identify input columns that are not useful and do not contribute significantly to the performance of neural network. We can remove insignificant inputs and improve the generalization performance of a neural network, in spite of losing some input information (Alyuda, 2003).

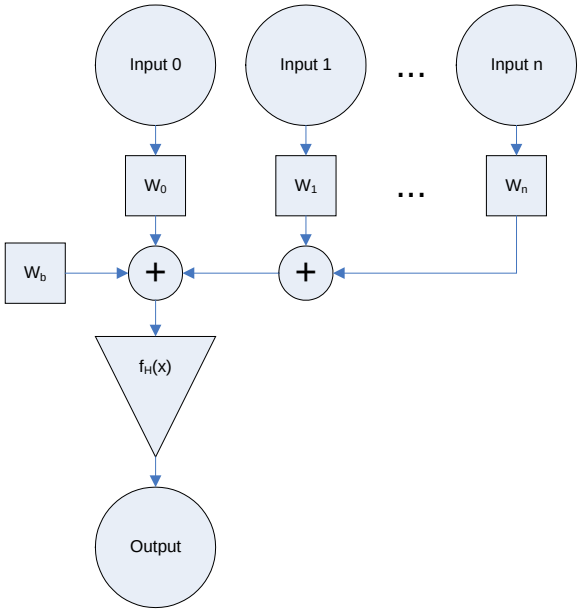

Figure 6: Basic processing elements of an ANN

In NeuroIntelligence you can use one of the following 4 methods of feature selection:

Forward stepwise, Backwards stepwise, Exhaustive search and Genetic algorithms. Details are given in Alyuda Manual (Alyuda, 2003).

All methods use generalized regression neural networks (GRNN) or probabilistic neural networks (PNN) because they train quickly and proved to be sensitive to the irrelevant inputs. NeuroIntelligence automatically uses GRNN for regression problems and PNN for classification problems.

The initial test network architectures were constrained to three layers, one for input, hidden and output layers, respectively. This architecture was chosen as previous research indicated that multiple hidden layers are rarely effective in terms of both accuracy and training speed, (Neocleous & Schizas, 2002).

The Training set is part of the input dataset used for neural network training, i.e. for adjustment of network weights. The Validation set is a part of the data used to tune network topology or network parameters other than weights. NeuroIntelligence uses Validation set to calculate generalization loss and retain the best network (the network with the lowest error on Validation set). The Test set is a part of the input data set used only to test how well the neural network will perform on new data. The Test set is used after the network is ready

(trained), to test what errors will occur during future network application. This set is not used during training and thus can be considered as consisting of new data entered by the user for the neural network application.
In this work, 68%, 16% and 16% of the data were selected for training, validation and test, respectively.
Because of the limitation of the number of data, exhaustive search was used to select the feature of the inputs. Logistic was selected for hidden layer and output activation FX, $1/(1+e^{-x})$. The most popular learning algorithms are back-propagation (BP) and its variants (Rumelhart, Hinton, & Williams, 1986). The training set has to be a representative collection of input-output examples. Back-propagation training is a gradient-descent algorithm. It tries to improve the performance of the neural-network by reducing the total error by changing the weights along its gradient.
With a small number of weights (usually, up to 300), Levenberg- Marquardt (LM) algorithm is efficient; and often performs considerably faster than other algorithms and finds better optima than other algorithms. But its memory requirements are proportional to the square of the number of weights, which is not an issue here. There are seven different algorithms in the NeuroIntelligence to train the network. The LM and BP were compared before selecting either of them. For this work, The Levenberg-Marquardt algorithm was selected as training algorithm because it always produced better R^2 –values (closer to one). To compare the back-propagation and Levenberg-Marquardt algorithms in training, the B0, B1, B1* and B0* shown in the Table 2 are noticeable. As shown in the table, $2.5x10^5$ epochs in BP (B0*) gives almost the same performance as LM with 52 iterations does. Comparison of the number of iterations of B1 and B1* reveals that BP with 10^5 epochs even cannot perform as well as LM with 203 epochs.
Automatic feature selection was tried. After 511 iterations, these columns out of nine were rejected: y, y/H, T, P, and Ra. Because this selection, intuitively, doesn't make sense, therefore, automatic feature selection was overwritten; and manual selection was used. The training of all patterns of a training data set is called an *epoch* or *iteration*. Figure 7 shows the process map of this artificial neural networking.

SIMULATION

The following set of data was selected as an input to NeuroIntelligence: type of the wall (h for hot and c for cold wall), y (height from bottom of the cavity as Figure 1 shows), y/H, spacing (W), cold wall temperature (T_c), hot wall temperature (T_h), room temperature (T), room pressure (P), (T_h - T_c), diagonal symmetry (DS), and Rayleigh number (Ra). Because of a physical limitation on the height of the interferometer beam, the measurements were made only

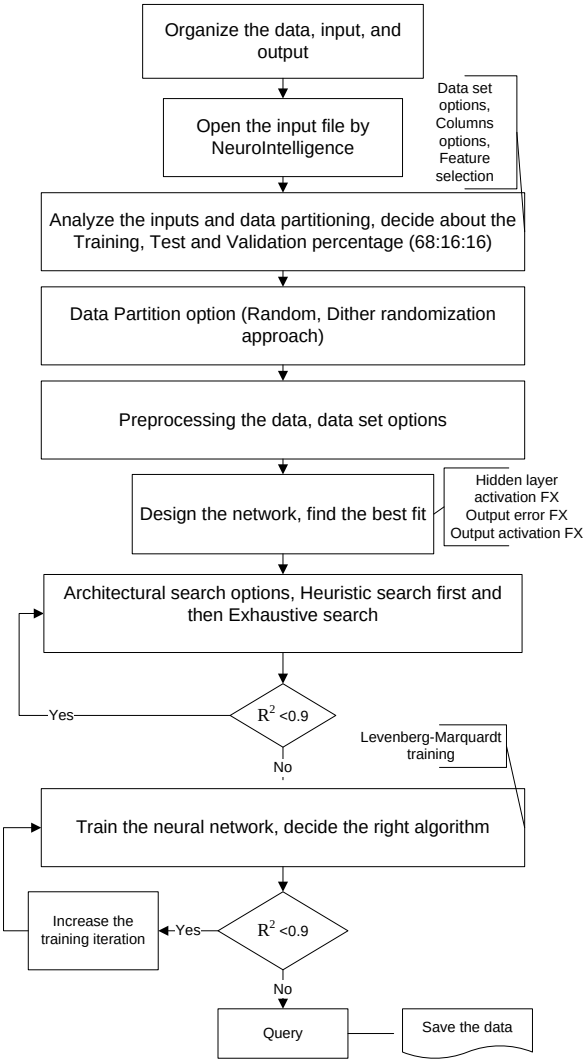

Figure 7: Process map of the ANN to predict the local Nu

in the bottom half of the cavity ($0 \le y/H \le 0.5$). It would have been difficult to raise the 350 kg optical bench safely to the height required to make measurements in the upper half. Nevertheless, it was still possible to compute the local timed-averaged Nusselt number, using the assumption of "diagonal symmetry" (DS). In this case (DS), measurements on the lower half of the hot wall is considered as the values for upper half of the cold wall diagonally, i.e., new y = H – measured y. Room temperature and pressure are not directly related to Nusselt number calculation, they are measured, practically, to adjust the cold and hot temperature heat bath and to calculate the air properties inside the cavity. Air is considered an ideal gas. The temperature difference between cold and hot plate has a direct impact on Nusselt number. Considering the above points some sets of inputs are designed. Table 1 shows the network names (Net#) and their inputs.

Time-averaged local Nusselt number (Nu) was given to the ANN as target. Later, inputs were refined to see their effects on the target prediction. In the table, letter "A" means all the above raw data for different sizes were used as inputs. The inputs are entered to ANN as they were measured without and manipulation or adjustments. DS stands for *diagonal symmetry* and isn't an input, but describes the type of input for y-value. Letter "B" refers to the data that are classified. In this classification, only the largest cavity (W = 56) is employed and other sizes data were rejected. Air flow inside this cavity is fully turbulent, chaotic and 3-D (Poulad, 2009). Any discrete values would be considered as "Category", even if they are number. In network B2,ΔT is inputted as "Category" or "C", which is not interpreted as number. It consists of 12 categories (i.e., 15, 15.1, 15.2, up to 15.12). That is why the input number is 15 for B2 network in Table 2, i.e., 12 categories plus 3 numbers. To see the effect of "Categorization", the network B3 was designed with ΔT as number. Spacing (W) and wall type are always categorized as "C". The former is composed of 5 (i.e., 12.7, 32.3, 40, 56.2, and 56.5) and the latter is composed of two categories (i.e., c and h).

Table 1: Different network names and their respective inputs (B refers to the size W = 56 data only)

Net#	Inputs
A0	Wall type, W, y, y/H, T_c, T_h, T, P, Ra
A1	DS, W, y, y/H, T_c, T_h, T, P, Ra
A2	DS, W, y, y/H, ΔT, T, P, Ra
A3	DS, W, y, y/H, ΔT, Ra
A4	Wall type, W, y, y/H, T_c, T_h, Ra
A5	DS, W, y, y/H, T_c, T_h, Ra
B0	Wall type, y, y/H, T_c, T_h, T, P, Ra
B1	DS, y, y/H, T_c, T_h, T, P, Ra
B2	DS, y, y/H, ΔT as "C", Ra
B3	DS, y, y/H, ΔT, Ra
B4	DS, y, y/H, , T_c, T_h, Ra

In Table 2, the best fit structures and the related testing R^2 are summarized. The closer the R^2 parameter to 1 the better the network is. The best fit- R^2 is related to the structure of the network; and the test- R^2 shows how well the training process was.

To determine the number of hidden neurons the network should have to perform its best, one are often left out to the method trial and error. If the hidden number of neurons are increase too much it will get an over fit result, that is the net will have problem to generalize. The training set of data will be memorized, making the network useless on new data sets. If the number of the neurons is not enough, network is unable to learn problem concept. Therefore, to estimate the number of hidden neurons, the network was run with different number of hidden neurons. Figure 8 shows the effect of structure on R-square and correlation. It was done on a nine input data set to find the best structure. It shows that one hidden layer perform better than two. Also, correlation value is always bigger than R^2-value. Based on this preliminary test, three-layer structure was selected for this work.

Table 2: Different networks structures to input ANN

Network	Structure	Best fit-R^2	Test-R^2	# of epoch
A0	13-17-1	0.993	0.981	82
A1	12-26-1	0.931	0.917	51
A2	11-18-1	0.974	0.914	40
A3	9-14-1	0.973	0.966	22
A4	11-13-1	0.997	0.988	20
A5	10-24-1	0.995	0.989	13
B0	8-5-1	0.995	0.978	52
B0*	8-5-1	0.995	0.992	2.5e5
B1	7-14-1	0.997	0.998	203
B2	15-7-1	0.961	0.932	300
B3	4-18-1	0.985	0.987	10
B4	5-19-1	0.998	0.997	206
B1*	7-14-1	0.997	0.985	10^5

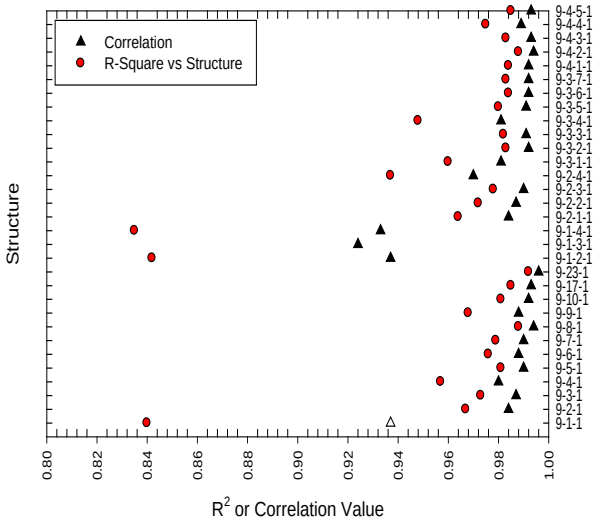

Figure 8: Effects of structure on the R^2 and correlation.

ANALYSIS

Data are partitioned as: Training set (68.66%), Validation set (15.67%) and Test set (15.67%). The statistical coefficient of multiple determinations (R^2-value) obtained for comparing the performance of each structure. To compare the performance of different networks, this experiment result is used:

y = 263.4, y/H = 0.269, W = 56.7, T_c = 13.24, T_h = 28.3, T = 23.5, ΔT = 15.06, P = 758 and Ra = 2.8×10^5. The calculated (actual) value for local time-averaged Nusselt number was $2.94 \pm 5\%$. That measurement is the most valid measurement for Nu because it is the

average of three set of measurements, each contained 2000 interferograms.

Table 3 summarizes the deviation from actual value of different networks. A1 provide the worst prediction. A2 is almost the same. A3 and A4 performances show that T and P could be omitted from the inputs. Comparison of the percent deviation of A-type with B-type networks reveals that classification of the data based on the size (W) of cavity is advisable. On the other hand, manipulation of input data in neural networking is not recommended. Data should be inputted as they are monitored or measured. That leads the analysis to see the share of each size into the ANN inputs. Table 4 shows that size 56 has about 46% sharing into the ANN. Analysis of B-type networks performance also implies that about 60 experiments suffices for each size to input the ANN. Moreover, error-value of B2-which is the worst amongst of all B-type networks- implies that categorization $\Delta$of misleads the NeuroIntelligence software.

Table 3: Performance of different networks

Network #	Nu Prediction	%Deviation
A0	2.74	7
A1	2.31	27
A2	2.41	22
A3	3.21	8
A4	2.96	1
A5	3.08	5
B0	2.89	2
B1	2.85	3
B2	2.72	8
B3	2.91	1
B4	3.11	5

Table 4: Share of different size in ANN input

Size (W in mm)	# of inputs	% of share
12.7	28	20.9
32.3	25	18.7
40	20	14.9
56.2	61	45.5
Total inputs	134	100

Figure 9 shows how well training of the network was done. This is the scatter plot of network B4. Outputs of the training (dots) are very close and uniformly scattered around targets (line). That is, how well the trained network can predict the outputs in testing data.

Figure 10 presents the plots of Nusselt number versus y/H, which was predicted by network B4 (triangles) and values calculated from experiment measurements (solid-line connected circles). y/H is one of the inputs given to the trained network to find the Nu along the cold wall through the neural network. As the last row of table 3 shows, the network is about 5% different from the actual value. This uncertainty, on the average, goes to all Nu number values in the Figure 10. On the other hand, the trend of the heat transfer is well matched with the experimental findings. On the cold wall, there is no convective heat transfer at the bottom, but at the top, the convection is the maximum due to impingement of the hot air to the surface in this region. Along this wall, middle region has almost uniform convection.

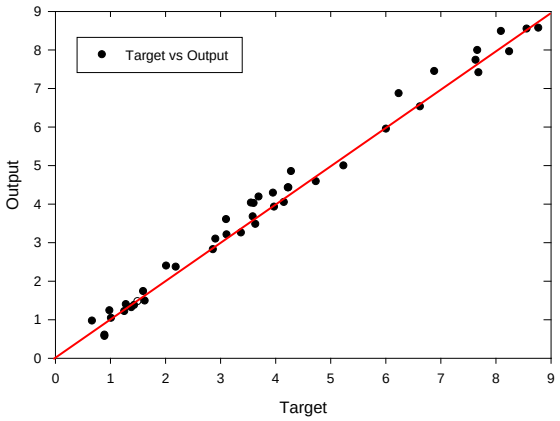

Figure 9: Scatter plot of training network B4.

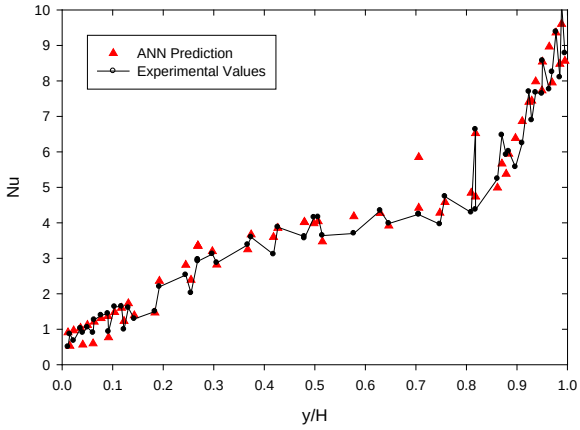

Figure 10: Results graph of the network B4.

RESULTS

Any calculation of raw data or manipulation on them is not helpful for better forecast by the ANN. For example, as Figure 11 shows, applying diagonal symmetry or substitutingΔT instead of cold wall and hot wall temperatures does not lead to better predictions. Another implication of better performance of B-type networks is that at least 60 experiments per 100 mm (H in Figure 1) should be implemented to train the ANN properly. It translates a minimum of 6 measurements in each centimeter of the cavity height (H). Even with small set of data, the ANN uncertainty

is about the uncertainty of exact calculation backed up by accurate experimental measurements. They are both found to be around %5 uncertain.

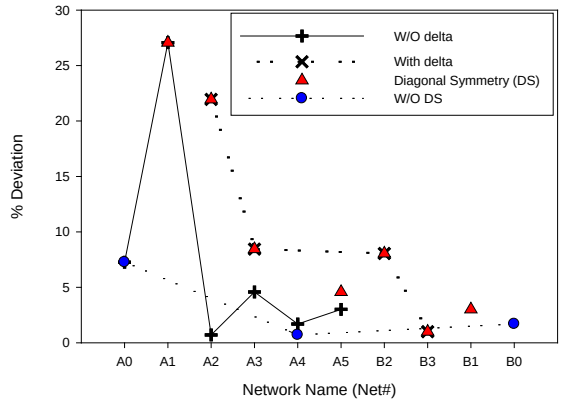

Figure 11: Performance of different networks (delta refers to ΔT)

The ANN was trained with the data from all experiments, but one of the most accurate one (exp. # 145). This was used later to check the validation of trained NN. It turned out the uncertainty was about %5. This is about the same uncertainty in experimental measurements. After validation, random values for y/H were queried (Figure 10). It matched with trend of Nusselt number along the cold wall, which was found experimentally.

CONCLUSIONS

Time-averaged local Nusselt number in a tall vertical cavity was measured in different elevations using a combination of MZI and high speed cinematography. Then an ANN was developed and trained based on the experimental measurements. Finally, the trained neural networks were used to predict the local Nusselt numbers of the largest cavity size (56) along different height. The application presented here is neither complete nor perfect, but merely a sample that demonstrates the usefulness of artificial neural-network. Based on the work presented here, it is believed that ANNs offer an alternative method to predict the local Nu number in the cavity which should not be underestimated. More experiments have yet to be done and feed to NN if the more accurate predictions are required. This work shows that ANN is as good as experimental results in finding the local time-averaged heat transfer. That means a well-trained ANN can be used to predict local heat transfer to build more accurate building energy simulation programs.

ACKNOWLEDGEMENTS

This work was funded in part by the Solar Buildings Research Network under the Strategic Network Grants Program and Discovery Grant of the Natural Sciences and Engineering Research Council (NSERC) of Canada.

REFERENCES

Abodahab, N., & Muneer, T. (Feb. 1998). Free convection analysis of a window cavity and its longitudinal temperature profile. *Energy Conversion and Management* , 39 (3-4) 257-267.

Alyuda. (2003). User Manual Version 2.1. Alyuda Research Inc.

Aydinalp, M., Ugursal, V. I., & Fung, A. S. (2003). Modelling of residential energy consumption at the national level. *International Journal of Energy Research* , 27:441–453.

Gouda, M., Danaher, S., & Underwood, C. (2002). Application of an artificial neural network for modelling the thermal dynamics of a building's space and its heating System. *Mathmatica and Computer Modelling of Dynamical Systems* , 8 (3) 333-344.

Kalogirou, S., & Bojic, M. (2000). Artificial neural networks for the prediction of the energy consumption of a passive solar building. *Energy—The International Journal* , 25(5):479–91.

Neocleous, & Schizas. (2002). Artificial neural network learning: a comparative. *LNAI* , 2308 300-313.

Poulad, M., Naylor, D., & Oosthuizen, P. (June 25–27, 2009). 'Measurement of unsteady convection in a complex fenestration using laser interferometry. *Canadian Solar Buildings Conference*, (pp. 139-148). Toronto, ON.

Ravindranath, G., Prabhukumar, G., & Devaru, B. (2007). Application of an artificial neural network in gas-solid (air-solid) fluidized bed: Heat transfer predictions. *ASME International Mechanical Engineering Congress and Exposition* (p. 8). ASME.

Rumelhart, D., Hinton, G., & Williams, R. (1986). Parallel Distributed Processing Explorations in the Microstructure of Cognition . In *Learning internal representations by error propagation* (pp. Vol. 1., Chapter 8). Cambridge (MA): MIT Press.

Wright, L. J. (1998). Simplified numerical method for assessing the condensation resistance of windows. *ASHRAE Transactions* , 104 (Pt 1B) 1222-1229.